PROCEEDINGS of the
23rd International Congress on Acoustics

9 to 13 September 2019 in Aachen, Germany

A model of the prespike at the calyx of Held synapse.

Martijn C. SIERKSMA[1,2]; J. Gerard G. BORST[1]

[1] Erasmus MC, Rotterdam, The Netherlands

[2] Institut de la Vision, Paris, France

ABSTRACT

The calyx of Held synapse is a giant axosomatic synapse in the brainstem that functions as a fast and reliable auditory relay. Because of its large size, the presynaptic action potential can be picked up in a recording of the postsynaptic cell. This so-called prespike is caused by the ephaptic coupling of presynaptic membrane currents via the synaptic cleft. We constructed an electric model of the prespike and estimated values for the leak conductance of the synaptic cleft, the capacitance of the release face and the presynaptic calcium current density based on simultaneous pre- and postsynaptic voltage clamp recordings. These values allowed us to estimate an impact of presynaptic capacitive and ionic currents on the cleft potential, and suggested that fenestration of the calyx of Held during development might be important to further reduce the cleft leak conductance of the cleft to minimize its impact on the presynaptic calcium channels.

Keywords: Ephaptic coupling, Synaptic transmission, Calyx of Held

1. INTRODUCTION

The calyx of Held synapse is a fast and reliable relay in the auditory brainstem. It forms between a globular bushy cell and a principal neuron of the medial nucleus of the trapezoid body. Each principal neuron is typically contacted by a single, giant, axosomatic terminal called the calyx of Held. The accessibility of this giant terminal for patch-clamp slice recordings has allowed it to become a model system for studying mammalian synaptic transmission (1). During whole-cell patch clamp recordings of the principal neurons a prespike can be detected, which reflects the presynaptic action potential (AP) (2). This prespike is an example of ephaptic synaptic coupling (3), as it is generated by presynaptic membrane currents involved in calyceal AP generation leading to a change in the cleft potential, which is then detected in the postsynaptic cell. The shape of the prespike can thus be informative about the shape of the intracellular calyceal action potential and the local presynaptic membrane currents flowing at the release face. Indeed, analysis of the *in vivo* shape of the prespike has been used to infer differences in calyceal spike depression in a mouse model for the neurodevelopmental disorder Angelman syndrome (4). However, despite the wealth of knowledge about the calyceal AP and its underlying voltage-dependent ion currents, the relation between the postsynaptically recorded prespike waveform and the presynaptic ion currents during the calyceal AP has not yet been studied. Here, we therefore revisit simultaneous voltage clamp recordings from the calyx of Held and its postsynaptic target (5) to evaluate the generation of the prespike. These recordings helped to define a simple biophysical model of the prespike and to better delineate the electrical properties of the synaptic cleft and the subcellular localization of presynaptic ion channels.

2. METHODS

2.1 Recordings

Simultaneous presynaptic current clamp and postsynaptic voltage clamp recordings from the rat MNTB (Figure 1A) were originally described in refs. (6, 7). The simultaneous pre- and postsynaptic voltage clamp recordings were originally described in ref. (11). Except for some details not provided in the Methods sections of these papers, we therefore refer to them for experimental details. Recordings were corrected for a 0.1 ms difference in delay due to differential filtering (10 kHz for presynaptic current clamp recordings and 3 kHz for postsynaptic voltage clamp recordings). The second derivative of the presynaptic action potential waveform (APW) command was filtered to 1.5

kHz with a Gaussian filter to better match the recorded postsynaptic signal. To minimize interference by the EPSCs evoked by the presynaptic calcium currents, we used the last 30 stimulations of a 50 APW train. At the stimulation rate of 100 Hz, the EPSCs evoked by these stimuli were substantially depressed. The bi-exponential fit of the decay of the preceding EPSC was subtracted from the postsynaptic currents. The remaining current, which we call the active prespike, was averaged. The passive prespike was estimated by summing the presynaptic P/5 stimulations.

2.2 **Model**

Inspired by a published model (8), we designed an electrical circuit model to mimic the current flow underlying the postsynaptically recorded prespike at the calyx of Held synapse (Figure 1B). We assumed that the prespike is generated exclusively by currents that flow through the synaptic cleft. According to Kirchhoff's first law, the current that flows from the presynaptic release face into the cleft must be equal to the sum of the current that leaks out of the cleft and the current that flows into the postsynaptic cell. The presynaptic current consists of a capacitive current across the capacitance contacting the synaptic cleft (c_{pre}) and the currents via ion channels (I_{ch}), which includes voltage-gated sodium channels (VGSCs), voltage-gated high-threshold potassium channels (HTKs), voltage-gated low-threshold potassium channels (LTKs) and voltage-gated calcium channels (VGCCs). The current can escape the cleft via an ohmic leak conductance (g_{leak}) or enter into the postsynaptic cell via the membrane capacitance that is in contact with the synaptic cleft (c_{cp}) or via a synaptic conductance (g_{syn}). The changes in the cleft potential (V_{cl}) will have an impact on the capacitive currents, on the driving forces of the conductances and on the voltage-dependent channel kinetics. The ionic current from the synaptic cleft into the postsynaptic cell is assumed to have a reversal potential of 0 mV. This will give us two differential equations, one for the synaptic cleft:

$$\left(c_{pre}+c_{pc}\right)\frac{dV_{cl}}{dt}=c_{pre}\frac{dV_{pre}}{dt}+c_{pc}\frac{dV_{post}}{dt}-g_{leak}V_{cl}-g_{syn}\left(V_{cl}-V_{post}\right)-\sum I_{ch} \qquad (1),$$

and one for the postsynaptic cell, which includes a resting conductance (g_{post}) that sets its resting membrane potential (V_{rest}) :

$$c_{post}\frac{dV_{post}}{dt}=c_{pc}\frac{dV_{cl}}{dt}-g_{syn}\left(V_{post}-V_{cl}\right)-g_{post}\left(V_{post}-V_{rest}\right) \qquad (2).$$

We assumed throughout that the presynaptic and postsynaptic capacitance facing the cleft were equal. These capacitances were calculated from the surface area by multiplying their contact area with the specific membrane capacitance (C_m). Values of the parameters for each model are listed in Table 1. Models for VGSCs, HTKs and LTKs were taken from ref. (9). Maximal conductance densities were 5.8 nS μm^{-2} and 0.7 nS μm^{-2} for g_{HTK} and g_{LTK}, respectively (9). The sodium channel density was adjusted to generate a 10 nA peak current with our AP template (10), and this conductance was distributed over 20 pF, giving a density of 0.4 nS μm^{-2}. For the VGCCs we used the Hodgkin-Huxley model described by ref. (11) for the calyx of Held. Maximal conductance was adjusted to generate a charge transfer of 1 or 0.75 pC and was 0.12 or 0.09 nS μm^{-2}, respectively. The model values correspond to room temperature kinetics. In all simulations, the postsynaptic resting potential was set to -70 mV, and the Nernst potentials for Na^+, K^+ and Ca^{2+} were set to +50, -90 and +40 mV, respectively. Changes in V_{cl} were taken into account when calculating the driving force. Total postsynaptic capacitance (c_{post}) was 25 pF, g_{post} was 4 nS and g_{syn} was 0 nS. Contact area to the cleft was set to 520 μm^2 and cleft leak conductance was set to 0.83 µS unless they were varied to assess their contribution. These values give a cleft time constant of 6 µs and a transfer constant of 0.03 fA V^{-1} s^2, which was in the same range as the experimental values.

Presynaptic APs were simulated using the same AP template that was used to elicit presynaptic calcium currents, unless noted otherwise. To calculate the transfer constant from our simulations, we changed the timing of the AP template to have a second derivative peak value of 1.67, 2.00, 2.32, 2.65 and 3.17 MV s^{-2}. The slope from the line fit between the AP'' peak values and the maximal postsynaptic response was used as the transfer constant (Figure 2B). Line fits were always near-perfect ($r > 0.999$). To estimate the time constant, the AP template for presynaptic calcium currents was used to simulate the calcium current and the postsynaptic prespike with the only-VGCCs-model at a density of 0.11 nS μm^{-2}. The passive prespike was simulated using the capacitive-only model. The time constant was estimated as shown in Figure 2E for an experimental example.

Differential equations were numerically solved using the function IntegrateODE of Igor Pro 6.37 (Wavemetrics) at its default settings. Channel states were initialized at the values reached after 3 ms at the first point of V_{pre}.

Data are presented as mean ± standard deviation.

Table 1. Default model parameters for simulations.

		Homogen.	No VGSCs	Only VGCCs	Cap.-only	
Max. VGSC conductance	g_{Na}	0.65	0	0	0	nS µm^{-2}
Max. HTK conductance	g_{HTK}	5.8	5.8	0	0	nS µm^{-2}
Max. LTK conductance	g_{LTK}	0.7	0.7	0	0	nS µm^{-2}
Max. VGCC conductance	g_{Ca}	0.09	0.09	0.09	0	nS µm^{-2}

3. RESULTS

3.1 An electrical circuit that generates prespikes

As the prespike is generated by currents that flow from the calyx to its target neuron, we simulated an electrical circuit *in silico* consisting of the terminal's release face, a synaptic cleft that is isolated from the reference by a leak conductance, and a passive neuron that partly faces the synaptic cleft. We did not include a resistive connection between calyx and target since capacitive currents are likely to dominate the postsynaptic currents during the prespike: the admittance for 500 Hz across an area of 1000 µm^2 is 31 nS ($2\pi f C_m A$), which is much larger than the postsynaptic resting conductance of 4 nS, while no physiological evidence for gap junctions (12) has been found at the calyx of Held synapse. The model is illustrated in Figure 1. If we disregard any currents through presynaptic ion channels facing the release face, the cleft potential should be proportional to the presynaptic capacitive current, which is proportional to the first derivative of the presynaptic AP waveform (AP'). In voltage clamp, the currents during the prespike will be dominated by capacitive currents, which are proportional to the first derivative of the cleft potential. Under these conditions, the prespike should therefore match the scaled, inverted second derivative of the presynaptic AP.

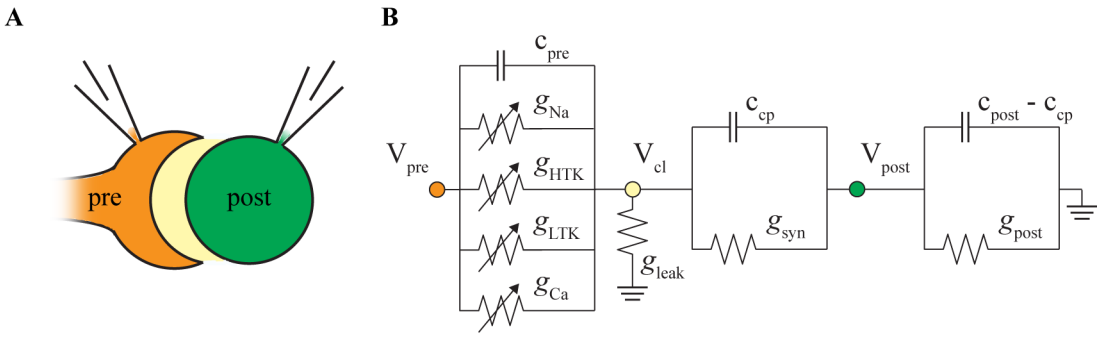

Figure 1 – Model circuit to simulate the prespike. (A) Drawing of the calyx of Held synapse. The calyx of Held terminal ('pre') covers a large area of the soma of its target neuron ('post'). In between is a small space, called the synaptic cleft, where membrane currents will flow during a presynaptic AP. (B) An electrical circuit for the capacitive and resistive currents that flow from the presynaptic membrane into the postsynaptic cell to generate a prespike.

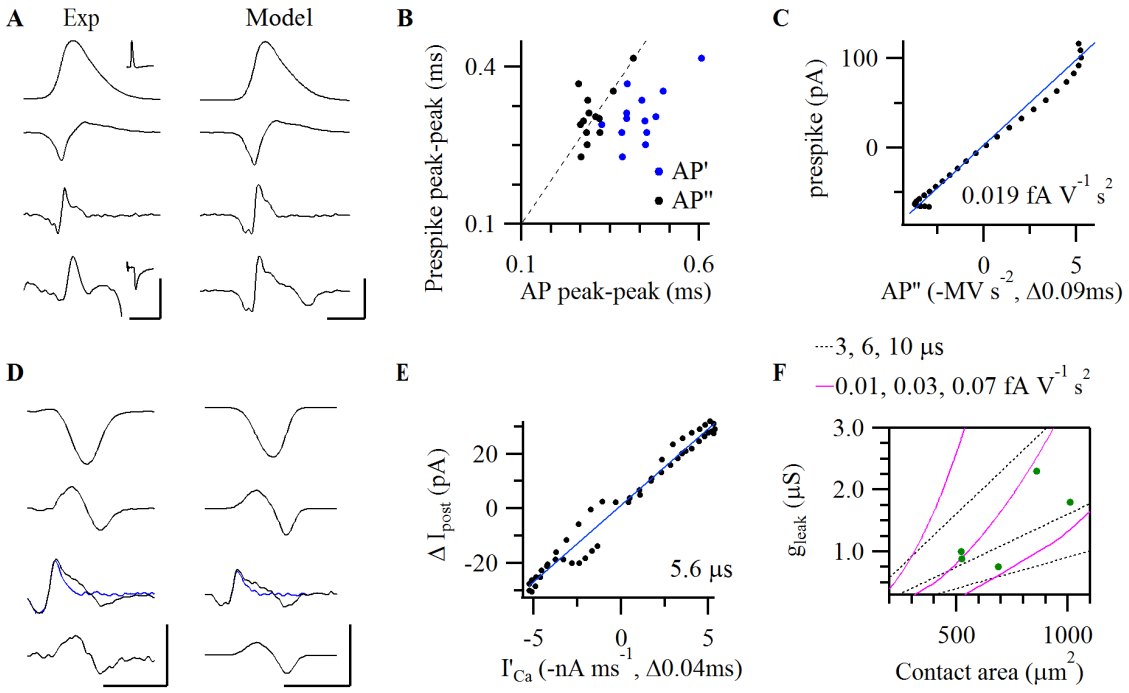

Figure 2 – Relation between the calyceal AP and the prespike. (A) *Left column, from top to bottom*: AP recorded from the calyx of Held, inverted first and second derivatives, and postsynaptic voltage clamp recording showing the accompanying prespike. Insets show on a longer time scale the same presynaptic AP (top) and the postsynaptic EPSC (bottom) elicited by the calyceal stimulation. *Right:* Only VGCCs-model results. Vertical scale bars (from top to bottom panels): 80 mV, 0.8 kV/s, 8 MV/s^2, 0.2 nA. Horizontal: 0.5 ms. (B) Relation between the delay between the first negative and positive peak of the prespike and the first two peaks in the first (blue) and second (black) derivative of the presynaptic AP. Dashed line is the identity line. (C) Relation between the prespike and the second derivative shown in A. Maximum correlation was obtained when delaying the second derivative by 90 µs. Blue line shows the regression line with a slope ('transfer constant') of 0.019 fA V^{-1} s^2. (D) *Left column, from top to bottom*: Presynaptic calcium current (after P/5 subtraction), its first derivative, postsynaptic currents (black) plus passive prespike (blue), difference between active and passive prespike. *Right*: corresponding model results. Vertical scale bars: 2 nA, 15 nA/ms, 0.15 nA, 0.1 nA. Horizontal: 1 ms. (E) Relation between the calcium component of the prespike and the first derivative of the presynaptic calcium current shown in D. Maximum correlation was obtained when delaying the first derivative by 40 µs. Blue line shows regression line with a slope ('time constant') of 5.6 µs. (F) Relation between the contact area and the cleft leak conductance for different values of the transfer constant (magenta lines) and the time constant (black lines). Green dots show the values of the model for the five double VC recordings calculated from the measured transfer and time constants. Calcium current density was 0.11 nS µm^{-2} in the simulations.

3.1 A comparison of the prespike with model predictions

We first looked at simultaneous whole-cell presynaptic current clamp recordings with postsynaptic voltage clamp recordings (6, 7). The afferent axon of the calyx of Held was stimulated with an electrode to trigger an AP, its corresponding postsynaptic prespike and an EPSC (Figure 2A). The prespike generally matched the scaled inverted second derivative of the AP (Figure 2A). Figure 2B shows that the time course of the second derivative of the AP indeed provides a better match for the prespike than its first derivative in these recordings (n = 13). From the relation between the second derivative of the AP and the prespike a transfer constant can be calculated (Figure 2C).

Next, we turned to simultaneous whole-cell pre- and postsynaptic voltage clamp recordings of the calyx of Held synapse that were originally reported in ref. (5), which were re-analyzed to compare them with model predictions. In these experiments the presynaptic compartment was voltage clamped with an APW command while the presynaptic calcium currents were pharmacologically isolated. A comparison of the second derivative of the APW and the prespike yielded a transfer constant of 0.04 ± 0.02 fA V^{-1} s^2 (n = 5) in these recordings.

3.2 Contribution of presynaptic calcium currents to the prespike

By subtracting the passive component from the postsynaptically recorded active prespike, a small current emerged that had a similar time course as the first derivative of the presynaptic calcium current (Figure 2D, left column). Its time course closely matched the model predictions (Figure 2D, right column). The amplitude of its positive peak was on average 56 ± 44 pA (n = 5). A comparison between the max rate of rise of the measured presynaptic calcium current and this peak provided a time constant (Figure 2E), which was on average 6.0 ± 2.0 µs. The combination of the transfer constant and the time constant provided an estimate for the contact area of the calyx, which was on average 730 ± 230 µm^2, and for the leak conductance of the synaptic cleft, which was on average 0.9 ± 0.4 µS. With these estimates we used the model to estimate the calcium conductances that would replicate the experimental results, which was on average 0.10 ± 0.06 nS µm^{-2}. To replicate the experimental changes the simulated V_{cl} peaked on average to 3.5 ± 0.6 mV, then reached a minimum of -3.2 ± 1.4 mV after which it returned to baseline. As expected, the calcium current did not affect the positive deflection of V_{cl} (Cap.-only model: 3.5 ± 0.6 mV), but did affect the V_{cl} after the peak (Cap.-only model: -1.3 ± 0.2 mV). This change in V_{cl} due to the calcium current is subsequently observed in the prespike.

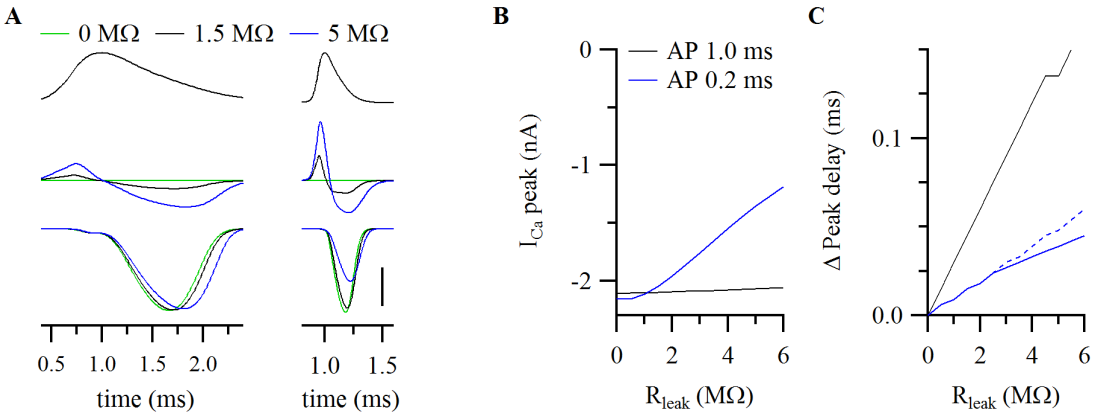

Figure 3 – Impact of the cleft potential on presynaptic calcium currents. (A) Simulation of the impact of a slow and a fast AP (top; FWHM: left 1.0, right 0.2 ms) on the cleft potential (middle) and the presynaptic calcium current (bottom) at three leak resistances, as indicated above the figure. Scale bar: 90 mV, 14 mV, 1nA. (B) Relation between peak calcium currents and leak resistance for the two APs. Driving force increases slightly (not shown). (C) The change in delay between the calcium peak current and the AP for the two APs (solid line). The dashed line shows the delay after correcting for the decrease in the calcium current shown in B. Calcium conductance density was 0.1 and 0.2 nS µm^{-2} for the slow and fast AP, respectively.

3.1 Impact of cleft potential on the presynaptic calcium currents

During development the presynaptic AP narrows from a half width of 0.5 to 0.2 ms (13). The briefer AP necessitates a much larger capacitive current, and may thus potentially result in a larger change in the cleft potential. As the voltage-dependent calcium channels at the release face sense V_{pre}-V_{cleft} instead of V_{pre}, their kinetics depend on the cleft potential. We simulated the consequences of the cleft potential on the calcium current by varying the cleft leak resistance (Figure 3). For a slow AP, the cleft potential changes to +2.5 mV and then to -3.8 mV for a leak resistance of 1.5 MΩ and a surface area of 520 μm^2. This causes a delay of 50 µs in the onset of the calcium current (Figure 3C), but has little effect on its size (Figure 3B). In contrast, with the faster AP we observe under the same conditions that the cleft potential changes to +11.4 mV and -5.9 mV. As a consequence, the peak calcium current is delayed by 30 µs and reduced by 25% (-0.86 vs -0.65 nA). The observed delay corresponds to the delay in reaching the $V_{pre} - V_{cleft}$ maximum compared to the V_{pre} maximum; the reduction is related to the smaller effective AP, which determines the maximal opening probability of the calcium conductance. We conclude that the developmental acceleration of the calyceal AP will increase the capacitive current to a level that would impede the opening of calcium channels if the synaptic cleft leak conductance remained unchanged.

3.2 Predictions for the contribution of other presynaptic ion currents to the prespike

The estimates for the cleft leak conductance and of the coupling for the calcium current allowed us to test the contribution of Na^+ and K^+ currents to the postsynaptically recorded prespike. We estimated their density based on literature values and assumed a homogeneous distribution within the terminal. Figure 4 illustrates that the presence of these channels at the release face would have a large impact on the shape and size of the prespike. Due to the gating differences, the timing of each current is different (Figure 4A), and thus their impact on the prespike as well (Figure 4B). A comparison with the recorded prespike (Figure 2A) suggests that it does not resemble the prespike of the homogeneous model, suggesting that some voltage-gated ion channels are excluded from the release face. Also, the impact of VGCCs on the prespike looks larger in our simulations than in the recorded prespikes. A more comprehensive comparison may allow an inference to what extent these channels are present at the release face.

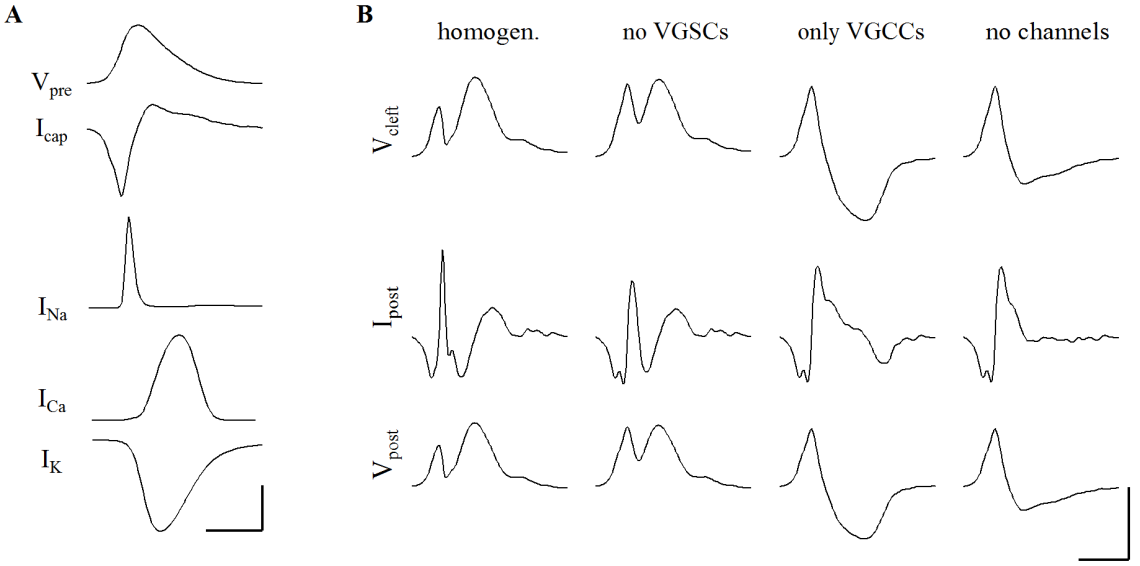

Figure 4 – Impact on the prespike of voltage-gated ion channels located at the release face. (A) Timing of different voltage-gated currents at the release face during the AP. Note that the amplitudes of each of the currents depend on cleft potential, thus creating a mutual dependency. Vertical scale bars: 60 mV, 2.4 nA, 1 nA, 1 nA, 3 nA. Horizontal: 0.5 ms. (B) The cleft potential (top), the VC prespike (middle), and the CC prespike (bottom) under different conductance density conditions. Homog.: homogeneous density; no VGSCs: no sodium conductance at the release face; only VGCCs: calcium and capacitive currents at the release face; no channels: the capacitive-only model. Scale bars: 4 mV, 0.2 nA, 1 mV.; 0.5 ms.

4. CONCLUSIONS

We studied a form of synaptic ephaptic coupling in which a fraction of the currents flowing at the presynaptic release face enter the postsynaptic cell to generate the prespike. By comparing model predictions and experiments in which both the presynaptic and the postsynaptic membrane currents could be measured, we could quantify the leak resistance of the synaptic cleft. The obtained value of ~1 MΩ is higher than the value of 0.3 MΩ assumed for the cerebellar pinceau synapse (8), but much lower than the value of at least 60 MΩ estimated for the synapse between cones and horizontal cells at the retina based on an ultrastructural reconstruction (14), or up to 3 GΩ assumed for the mossy fiber CA3 synapse (15). Our experiments were performed at room temperature in slices from pre-hearing rats, and most of the calyces probably still had a cup shape (16). Our simulations showed that under these conditions the impact of presynaptic currents on the cleft potential is modest. However, the speedup of the AP at physiological temperature and after hearing onset would increase this impact substantially. The large postsynaptic glutamate receptor current may also impact the cleft potential (17). We show that with the observed pre-hearing cleft leak resistance, the capacitive currents during the adult presynaptic AP may affect the timing and size of the presynaptic calcium current. Apart from the often mentioned facilitation of glutamate clearance (18-20) or the resistance against Ca^{2+} depletion (21), a lowering of the cleft leak resistance thus provides an additional argument for the desirability of the fenestration of the mature calyx.

Our model also allowed us to simulate the contribution of other voltage-dependent ion channels to the prespike. Interestingly, both sodium and potassium channels seem to largely avoid the release face in the mature calyx of Held (10, 22). A systematic comparison of modeled and measured prespikes may further delineate their contribution to changes in the cleft potential and its subsequent impact on the presynaptic action potential.

ACKNOWLEDGEMENTS

The research was supported by a grant from the Nederlandse Organisatie voor Wetenschappelijk Onderzoek – Aard- en Levenswetenschappen (#823.02006, ‘Development of a giant synapse’).

REFERENCES

1. Borst JGG, Soria van Hoeve J. The calyx of Held synapse: from model synapse to auditory relay. Annual Review of Physiology. 2012;74:199-224.
2. Forsythe ID. Direct patch recording from identified presynaptic terminals mediating glutamatergic EPSCs in the rat CNS, *in vitro*. J Physiol. 1994;479(3):381-7.
3. Anastassiou CA, Koch C. Ephaptic coupling to endogenous electric field activity: why bother? Curr Opin Neurobiol. 2015;31:95-103.
4. Wang T, van Woerden GM, Elgersma Y, Borst JGG. Enhanced transmission at the calyx of Held synapse in a mouse model for Angelman syndrome. Front Cell Neurosci. 2017;11:418.
5. Borst JGG, Sakmann B. Effect of changes in action potential shape on calcium currents and transmitter release in a calyx-type synapse of the rat auditory brainstem. Philos Trans R Soc Lond B Biol Sci. 1999;354(1381):347-55.
6. Borst JGG, Sakmann B. Calcium influx and transmitter release in a fast CNS synapse. Nature. 1996;383(6599):431-4.
7. Borst JGG, Helmchen F, Sakmann B. Pre- and postsynaptic whole-cell recordings in the medial nucleus of the trapezoid body of the rat. J Physiol. 1995;489(Pt 3):825-40.
8. Blot A, Barbour B. Ultra-rapid axon-axon ephaptic inhibition of cerebellar Purkinje cells by the pinceau. Nat Neurosci. 2014;17(2):289-95.
9. Yang YM, Wang W, Fedchyshyn MJ, Zhou Z, Ding J, Wang LY. Enhancing the fidelity of neurotransmission by activity-dependent facilitation of presynaptic potassium currents. Nat Commun. 2014;5:4564.
10. Leão RM, Kushmerick C, Pinaud R, Renden R, Li G-L, Taschenberger H, et al. Presynaptic Na^{+} channels: locus, development, and recovery from inactivation at a high-fidelity synapse. J Neurosci. 2005;25(14):3724-38.
11. Borst JGG, Sakmann B. Calcium current during a single action potential in a large presynaptic terminal of the rat brainstem. J Physiol. 1998;506:143-57.
12. Rubio ME, Nagy JI. Connexin36 expression in major centers of the auditory system in the CNS of mouse and rat: Evidence for neurons forming purely electrical synapses and morphologically mixed

synapses. Neuroscience. 2015;303:604-29.
13. Taschenberger H, von Gersdorff H. Fine-tuning an auditory synapse for speed and fidelity: developmental changes in presynaptic waveform, EPSC kinetics, and synaptic plasticity. J Neurosci. 2000;20(24):9162-73.
14. Fahrenfort I, Steijaert M, Sjoerdsma T, Vickers E, Ripps H, van Asselt J, et al. Hemichannel-mediated and pH-based feedback from horizontal cells to cones in the vertebrate retina. PLoS One. 2009;4(6):e6090.
15. Kasyanov AM, Maximov VV, Byzov AL, Berretta N, Sokolov MV, Gasparini S, et al. Differences in amplitude-voltage relations between minimal and composite mossy fibre responses of rat CA3 hippocampal neurons support the existence of intrasynaptic ephaptic feedback in large synapses. Neuroscience. 2000;101(2):323-36.
16. Kandler K, Friauf E. Pre- and postnatal development of efferent connections of the cochlear nucleus in the rat. Journal of Comparative Neurology. 1993;328(2):161-84.
17. Savtchenko LP. Bilateral processing in chemical synapses with electrical 'ephaptic' feedback: a theoretical model. Math Biosci. 2007;207(1):113-37.
18. Ford MC, Grothe B, Klug A. Fenestration of the calyx of Held occurs sequentially along the tonotopic axis, is influenced by afferent activity, and facilitates glutamate clearance. J Comp Neurol. 2009;514(1):92-106.
19. Taschenberger H, Leão RM, Rowland KC, Spirou GA, von Gersdorff H. Optimizing synaptic architecture and efficiency for high-frequency transmission. Neuron. 2002;36(6):1127-43.
20. Palmer MJ, Taschenberger H, Hull C, Tremere L, von Gersdorff H. Synaptic activation of presynaptic glutamate transporter currents in nerve terminals. J Neurosci. 2003;23(12):4831-41.
21. Borst JGG, Sakmann B. Depletion of calcium in the synaptic cleft of a calyx-type synapse in the rat brainstem. Journal of Physiology. 1999;521:123-33.
22. Elezgarai I, Díez J, Puente N, Azkue JJ, Benítez R, Bilbao A, et al. Subcellular localization of the voltage-dependent potassium channel Kv3.1b in postnatal and adult rat medial nucleus of the trapezoid body. Neuroscience. 2003;118(4):889-98.